

SIMPÓSIO 2012

MATERIAIS E PROCESSOS SUSTENTÁVEIS

LIVRO DE ACTAS

Unidade de Materiais Têxteis e Papeleiros

COVILHÃ, UNIVERSIDADE DA BEIRA INTERIOR
6-7 DE DEZEMBRO DE 2012

Reservados todos os direitos

Título:

Actas do Simpósio 2012: MATERIAIS E PROCESSOS SUSTENTÁVEIS
UMTP, Universidade da Beira Interior
6-7 de Dezembro de 2012, Covilhã - Portugal

Coordenador da Edição:

Manuel José dos Santos Silva

Comissão Organizadora:

Manuel José dos Santos Silva

Ana Maria Carreira Lopes

José Mendes Lucas

Rogério Simões

Álvaro Campos Vaz

Madalena Rocha Pereira

Maria José Pacheco

Ana Paula Costa

Carla Sofia Gaiolas

Isabel G. Trindade

Susana Ramos

Comissão Científica:

Manuel José dos Santos Silva

Ana Maria Carreira Lopes

José Mendes Lucas

Rogério Simões

Albertina Amaro

Madalena Rocha Pereira

Dina Mendonça

José Albertino Figueiredo

Ana Maria Ramos

Rui Miguel

Apoio Técnico:

Maria da Conceição Camisão

Execução Gráfica:

Serviços Gráficos da Universidade da Beira Interior

Tiragem:

550 exemplares

ISBN:

978-989-654-114-9

Depósito Legal:

366483/13

Apoios:



UNIVERSIDADE DA BEIRA INTERIOR
Covilhã | Portugal

FCT Fundação para a Ciência e a Tecnologia

MINISTÉRIO DA CIÊNCIA, TECNOLOGIA E ENSINO SUPERIOR Portugal



ÍNDICE

| | |
|--|----|
| Programa da Conferência / Conference Programme | 9 |
| Fabrics, modularity and technology in the development of fashion accessories: a step closer to sustainability, <i>L. Ribeiro, R. Miguel, M. Pereira, J. Lucas, I. G. Trindade</i> | 15 |
| Vestuário Técnico para o Quotidiano, <i>C. A. Lopes, M. J. Geraldês</i> | 19 |
| Etiquetas Têxteis com a Integração de Símbolos para Interpretação de Cores em Padrões pelos Daltónicos, <i>F. Craveiro, J. Lucas</i> | 21 |
| Contribution to the structural characterization of Nano Structured Polymeric Materials using a 3D Computational Simulation Model, <i>J. M. R. Curto, E. L. T. Conceição, P. A. F. Rodrigues, N. J. R. Belino, A. T. G. Portugal, R. M. S. Simões, M. J. S. Silva</i> | 25 |
| Sistema para análise da formação da folha de papel por retrodifusão e transmissão da radiação laser, <i>A. O. Mendes, P. T. Fiadeiro, M. V. Bernardo, A. P. Costa, M. E. Amaral, M. N. Belgacem</i> | 29 |
| Anaerobic treatment of olive mill wastewater: profile of sugars, organic acids and phenolic compounds, <i>L. R. Fernandes, A. Gomes, A. Lopes, R. M. Simões</i> | 33 |
| Influence of the experimental conditions on the electrodegradation of tetracyclines, <i>A. Fernandes, C. Oliveira, N. Monteiro, C. Brinzilla, M. J. Pacheco, L. Ciriaco, A. Lopes</i> | 37 |
| A new medical textile: L-cysteine functionalized cotton, its mechanism of action and potential antimicrobial properties, <i>M. Pedrosa, E. Caldeira, F. Silva, A. Oliveira, I. Gouveia</i> | 40 |
| Treatment of cork processing industrial effluent with an innovative system of Constructed Wetland and Ozonation, <i>Diana Santos, Williams Silva, Arlindo Gomes, Rogério Simões, Roberto Pascoal, António Albuquerque, Alexandros Stefanakis</i> | 46 |
| Conductive Textiles Functionalize with a Vapor Phase Polymerization Reactor, <i>J. Matos, I. G. Trindade, J. Lucas, R. Miguel, A. Rute, M. Magrinho, M. Pereira, M. Santos Silva</i> | 50 |
| Electrochemical techniques for pollution abatement in sanitary landfills, <i>E. Catalão, A. Fernandes, P. Luz, R. Simões, M. J. Pacheco, L. Ciriaco, A. Lopes</i> | 54 |
| DAPP as affinity ligand: support characterization and chromatographic studies with plasmid DNA, <i>Catarina Caramelo Nunes, Paulo Almeida, João C. Marcos, Cândida T. Tomaza</i> | 57 |
| Effect of continuous thermal stabilization process on thermal transitions and mechanical properties of a false-twist textured Polylactide multifilament, <i>A. M. Manich, M. Martí, J. Carilla, B. Baena, D. Cayuela</i> | 60 |

| | |
|---|-----|
| Estratégias e Práticas Sustentáveis em Empresas da Cadeia Têxtil, <i>M. Pereira, R. Miguel, J. Lucas, M. Santos Silva, I. Trindade</i> | 65 |
| Influence of ionic strength on the AO8 ionization, <i>M. J. R. G. Pires, M. I. A. Ferra, A. Marques</i> | 71 |
| Fabricação de materiais têxteis compósitos sustentáveis com matriz de <i>Hevea Brasiliensis</i> e reforço em malhas, <i>E. Garcia, M. J. Geraldês</i> | 74 |
| Ferrocene Derivatives with Potential Biological Activity, <i>S. Santos, J. A. Figueiredo, M. I. Ismael, A. C. Fernandes</i> | 78 |
| Synthesis and characterization of iminosugars, <i>M. Domingues, J. A. Figueiredo, M. Schuler, A. Tatibouët, M. I. Ismael</i> | 80 |
| Desenvolvimento de uma Ferramenta Electrotêxtil para Aferição da Qualidade do Sono através do Índice de Pittsburgh, <i>M. Tavares, N. Belino, M. Pato, M. J. Geraldês</i> | 82 |
| Antibacterial properties of some naturally occurring phenols against <i>Staphylococcus aureus</i> , <i>Â. Luís, A. P. Duarte, F. Domingues</i> | 86 |
| Preparation and Characterization of TiO_2/WO_3 nanocomposites films for photocatalytic applications, <i>L. C. Silva, M. E. Melo Jorge, S. Sérgio</i> | 90 |
| Photocatalytic degradation of Rhodamine 62G by nanocrystalline $\text{Ca}_{0.6}\text{Ho}_{0.4}\text{MnO}_3$ film under visible light, <i>B. Barrocas, A. Rovisco, Y. Nunes, S. Sérgio, M. E. Melo Jorge</i> | 94 |
| Antioxidant activity of solvent extracts from <i>Vitex agnus-castus</i> L., <i>Diogo Pereira, Carla Gaiolas, Jesus Rodilla, Rosalina Mata, Lúcia Silva</i> | 98 |
| Higher Education in Fashion Design - A Course of Research, <i>E. Lima, M. Calado, R. Miguel</i> | 100 |
| Natural Dyes: The benefits of Biotechnology and its application in textiles, <i>Gabriela da Cunha Santos, Cristina Carvalho</i> | 104 |
| Cold-plasma assisted grafting of cellulose fibers by acrylic monomers, <i>C. Gaiolas, M. E. Amaral, A. P. Costa, M. J. Santos Silva, M. N. Belgacem</i> | 110 |

POSTERS

| | |
|--|-----|
| New N-alkyl-2-alkylsulfanylacetanilide atropisomers: synthesis and VT NMR study, <i>S. S. Almeida, R. E. F. Boto, S. S. Ramos, P. Almeida</i> | 115 |
| Pulping Potential of <i>Ailanthus altissima</i> (Mill.) Swingle, <i>P. Baptista, A. P. Costa, M. E. Amaral, R. Simões</i> | 117 |
| Environmental applications of TiO_2 electrodes prepared by DC-Magnetron Sputtering, <i>S. Ferreira, S. Sérgio, M. E. Melo Jorge, L. Ciriaco, M. J. Pacheco, A. Lopes</i> | 121 |
| Heavy metals monitoring during the electrochemical treatment of municipal landfill leachates, <i>A. D. Fonseca, P. Spranger, A. Fernandes, L. Ciriaco, A. Lopes, M. J. Pacheco</i> | 125 |

| | |
|---|-----|
| Removal of Reactive Orange 16 by Biosorption, <i>C. Louro, I. Gonçalves, M. I. Ferra, H. M. Pinheiro</i> | 128 |
| Critical temperature and free energy of activation evaluation of new 2-alkoxy- <i>N</i> -alkylacetanilide atropisomers, <i>P. M. S. Leite, S. S. Ramos, R. E. F. Boto, P. Almeida</i> | 130 |
| Simulações de Antenas Têxteis, <i>C. Loss, R. Salvado, P. Pinho, R. Gonçalves</i> | 132 |
| Sesquiterpenes from <i>Croton gratissimus</i> , <i>L. I. N. Canelo, I. Mafuca, A. R. Estebainha, D. I. Mendonça, R. S. Mata</i> | 136 |
| Covalent and non-covalent strategies for surface modification of different textile materials with antimicrobial properties, <i>F. Nogueira, P. Teixeira, E. Piskin, I. Gouveia</i> | 137 |
| Malharia Funcional no segmento Infantil: O Body “Dry Baby”, <i>A. L. Olivete, M. J. Geraldês</i> .. | 139 |
| Sustainability in Fashion: Best Practices, <i>Madalena Pereira, Rui Miguel, Paulo Martins, Liliana Pina, Liliana Ribeiro</i> | 143 |
| Epoxidação do Guaiol e seus derivados, <i>Sofia Pombal, Jesus Rodilla, Lúcia Silva</i> | 144 |
| Trihalomethanes formation in treated wastewaters, <i>A. S. Rebelo, M. I. A. Ferra, R. Oliveira, A. Marques, I. Gonçalves</i> | 146 |
| Phenolic compounds in cork processing wastewater, <i>Diana Santos, Nicole Canto, Roberto Páscoa, Lúcia Silva, Rogério Simões, Arlindo Gomes</i> | 148 |
| Antioxidant activity of extracts from leaves of <i>Betula celtiberica</i> , <i>Ana Serra, Arlindo Gomes, Lúcia Silva</i> | 151 |

Electrochemical techniques for pollution abatement in sanitary landfills

E. Catalão, A. Fernandes, P. Spranger, R. Simões, M.J. Pacheco, L. Ciríaco, A. Lopes

UMTP and Department of Chemistry, University of Beira Interior, Covilhã, Portugal

Abstract

The anodic oxidation of leachate samples collected in a Portuguese municipal sanitary landfill was performed using as anode boron-doped diamond material. Two different experimental setups were tested: a batch reactor, with stirring, and a batch up-flow reactor with recirculation. Several different applied current densities were assayed, varying from 30 to 140 mA cm⁻². Although faster organic load removal is obtained at higher current density, the increase in current density also leads to a decrease in the current efficiency. However, to have significant removal rates in the organic or ammonium nitrogen, it is necessary to work with higher current densities and these parameters only start to decrease at an appreciable rate after most of the organic load, measured as chemical oxygen demand, is eliminated.

Introduction

Several types of pollutants can be found in sanitary landfill leachates composition, such as heavy metals, organic and inorganic compounds, some of them refractory and toxic [1-2]. The composition and concentration of the pollutants are influenced mainly by the nature of the solid wastes deposited, the climatic conditions and the age of the sanitary landfill [3-4]. One of the major problems in sanitary landfill leachate treatment is its low biodegradability. In fact, biological processes, the most commonly used to treat sanitary landfill leachates, have shown to have limited effectiveness when the ratio between the biological oxygen demand and the chemical oxygen demand, i.e., BOD₅/COD ratio, also known as biodegradability index, is lower than 0.5 [3].

Over the past 20 years, there are several studies reporting the application of technologies based on oxidation processes to eliminate colour, reduce the organic load and improve the biodegradability of sanitary landfill leachates [4-6]. Among the most promising electrochemical methods used in the wastewater treatment is the anodic oxidation [7,8].

Deng and Englehardt [6] present an overview of electrochemical oxidation processes used to treat landfill leachates. Although different materials are being used as anodes in the oxidation of persistent pollutants, the best results are obtained with boron-doped diamond (BDD) anodes, due to their unique chemical, electrochemical and structural stabilities that allow their use at high potentials, where most organic pollutants can be oxidized [9].

This way, the aim of this work was to evaluate the application of anodic oxidation, with BDD anode, to treat

leachate from an intermunicipal sanitary landfill, in order to fully fill the requisites that allow its discharge in the municipal wastewater treatment plant.

Materials and Methods

Leachate Characterization

The leachate samples used in this study were collected at a Portuguese intermunicipal sanitary landfill site before being submitted to any kind of treatment and the characteristics of the two different samples used are presented in Table 1. Besides the high COD content, the samples A and B have a ratio BOD₅/COD of 0.18 and 0.13, respectively, which points to an almost inexistent biodegradability. Also, TKN is very high and most of it is due to ammonium nitrogen.

Table 1. Characterization of the raw leachate samples used in this study.

| Parameter | Sample | |
|-------------------------|-------------|-------------|
| | A | B |
| COD (g/L) | 9.2 ± 0.7 | 8.3 ± 0.4 |
| BOD ₅ (g/L) | 1.7 ± 0.2 | 1.1 ± 0.4 |
| DOC (g/L) | 3.4 ± 0.1 | 3.3 ± 0.4 |
| TN (g/L) | 2.7 ± 0.1 | 2.7 ± 0.1 |
| TKN (g/L) | 2.4 ± 0.1 | 2.4 ± 0.2 |
| N-NH ₃ (g/L) | 2.2 ± 0.1 | 2.1 ± 0.3 |
| SS (g/L) | 0.7 ± 0.1 | -- |
| SD (g/L) | 16.6 ± 0.1 | -- |
| pH | 8.45 ± 0.05 | 8.21 ± 0.30 |
| Cond. (mS/cm) | 28.8 ± 1.2 | 29.4 ± 0.8 |

Electrochemical Experiments

Anodic oxidation (AO) experiments were conducted in two different cells: cell A, working in batch mode with stirring, having as anode a 10 cm² BDD plate and as cathode a 10 cm² stainless steel foil; cell B, working in batch mode with recirculation, having as anode a 20 cm² BDD plate and as cathode a 20 cm² stainless steel foil. The volume of raw leachate used in the experiments varied between 200 and 400 mL and assays were started at room temperature (25 ± 2 °C). However, during the assays the temperature can be naturally raised up to 45 °C. Several current densities were assayed, ranging from 30 to 140 mA cm⁻². A DC power supply GW, Lab DC, model GPS-3030D (0-30 V, 0-3 A) was used in the electrochemical experiments.

Analytical Methods

Degradation tests were followed by determinations, according standard procedures [10], of COD, BOD₅, Dissolved Organic Carbon (DOC), Total Nitrogen (TN), Total Kjeldahl Nitrogen (TKN), Total Ammonia Nitrogen (NH₃-N), Suspended Solids (SS) and Dissolved Solids (DS): COD determinations were made using the closed reflux titrimetric method; BOD₅ was measured by incubation for 5 days; DOC and TN were measured in a Shimadzu TOC-V CSH analyser and, before their determinations, the samples were filtrated through 0.45 µm glass microfiber filters; TKN and NH₃-N were determined using a Kjeldatherm block-digestion-system and a Vapodest 20s distillation system, both from Gerhardt. UV-Visible absorbance was measured from 200 to 800 nm using a Shimadzu UV-1800 spectrophotometer. pH was measured with a pH meter HANNA (HI 931400) and conductivity was determined using a conductivity meter Mettler Toledo (SevenEasy S30K).

Results and Discussion

For all the assays performed, the evolution in time of the COD was compared with the evolution of the theoretical COD, COD_{th}, determined according to the following equation [9]:

$$\text{COD}_{th} = \text{COD}_0 - \frac{8 \cdot I}{F \cdot V} t \quad (1)$$

where COD₀ is the initial COD, in mg/L, I is the current intensity, in A, F is the Faraday constant, 96485 C/mol, V is the volume of the sample, in m³, and t is the time, in s. Factor 8 relates the molar mass of O₂ (32 g) with electrons used in the oxidation of 1 mol of O₂ (4 e⁻). Bias between experimental COD and theoretical COD can be used to predict the current efficiency of the process.

Batch with stirring

In Figure 1 the results for the COD variation in time for the assays run at different current densities are presented. The figure also includes the theoretical COD, calculated according to equation 1, and we can observe that there is an increase in the bias between the theoretical and the experimental COD values with the current density, with a consequent decrease in the current efficiency.

In the assay run at 140 mA cm⁻² the anode area used was only 10 cm² and this is the reason why, apparently, the discrepancy between theoretical and experimental lines are similar to those from the assay run at 70 mA cm⁻². In fact, the intensity of the current in both assays, 70 and 140 mA cm⁻², is exactly the same and, since the experiments are performed in kinetic (current) control, the current efficiency should also be the same, which, in fact, can be observed in the Figure 1. This result is in agreement with the theoretical approach that, for the high COD of the samples, the assays are being run during most of the time in kinetic control, being the COD removal a function of the electrical charge that is provided to the reacting system.

The absolute removals in the various parameters used to follow the assays, after 6 h, are presented in Table 2. For the assays run between 50 and 100 mA cm⁻², and despite the decrease in current efficiency with current density, there is an increase in the removal of all the parameters. Regarding 140 mA cm⁻² assay results, and although the previous reasoning that pointed to removals similar to those of the assay run at 70 mA cm⁻², there is a big increase in all the parameters related with nitrogen removal, showing that the removal of the different nitrogen forms is very sensitive to the current density, instead of what happens with COD that is sensitive mainly to the electrical charge.

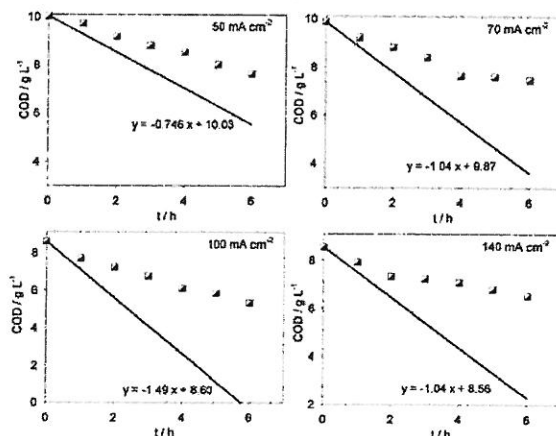


Figure 1. COD decay with time for the assays performed with cell A at different current densities: points – experimental; lines – theoretical.

Table 2. Absolute removals after 6 h assay for the experiments run with cell A, in batch with stirring mode at different current densities.

| Parameter | Current density / mA cm ⁻² | | | |
|---|---------------------------------------|------|------|------|
| | 50 | 70 | 100 | 140 |
| COD / mg L ⁻¹ | 2379 | 2417 | 3256 | 2030 |
| DOC / mg L ⁻¹ | 647 | 863 | 969 | 476 |
| TN / mg L ⁻¹ | 497 | 677 | 862 | 1040 |
| TKN / mg L ⁻¹ | 220 | 860 | 950 | 1148 |
| N-NH ₃ / mg L ⁻¹ | 527 | 867 | 1085 | 1022 |
| BOD ₅ / mgO ₂ L ⁻¹ | 554 | —* | —* | —* |

* not determined.

Up-flow batch with recirculation

The results obtained in the cell B, working in up-flow batch with recirculation mode, are presented in Figure 2 and Table 3. The general conclusions that can be drawn from their observation are, in general, very similar to those gathered with the assays run with cell A. Only the assay run at 50 mA cm⁻² shows a COD decay with "irregular" performance that exceeds the tendency line predicted by equation 1. The removals of the nitrogen compounds are very good, although always lower than COD removals.

Regarding current efficiencies, they are close to 100 % in the assays performed at lower current densities and, even at 100 mA cm⁻², it is very high.

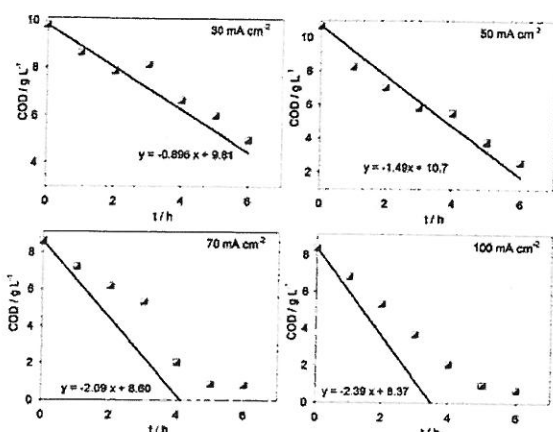


Figure 2. COD decay with time for the assays performed with cell B at different current densities: points – experimental; lines – theoretical.

Table 3. Absolute removals after 6 h assay for the experiments run with cell B, working in batch with recirculation mode at different current densities.

| Parameter | Current density / mA cm ⁻² | | | |
|--|---------------------------------------|------|------|------|
| | 30 | 50 | 70 | 100 |
| COD / mg L ⁻¹ | 4835 | 8097 | 6870 | 7674 |
| DOC / mg L ⁻¹ | 1676 | 2458 | 2355 | 2667 |
| TN / mg L ⁻¹ | 80 | 777 | 770 | 1074 |
| TKN / mg L ⁻¹ | 241 | 624 | 1057 | 1668 |
| N-NH ₃ / mg L ⁻¹ | 551 | 711 | 837 | 1211 |
| BOD ₅ / mg O ₂ L ⁻¹ | 415 | --* | --* | --* |

*not determined.

Conclusions

From this study the following conclusions can be drawn:

- Anodic oxidation with BDD anodes can, definitively, be an alternative to treat effluents as difficult as leachates from sanitary landfills are.
- For the experimental conditions tested and for both experimental setups, an increase in the current density leads to an increase in the organic load removal rate. However, it also decreases the current efficiency.
- For equal current density, COD removal rate is higher when cell B is used, i.e., the hydrodynamic in the cell with recirculation is more effective in the oxidation process.
- The removal of the nitrogen compounds increases with current density and their removal is more effective when COD becomes low.

References

1. Öman, C.B., Junestedt, C., 2008. Chemical characterization of landfill leachates – 400 parameters and compounds. *Waste Manage.* 28, 1876-1891.
2. Eggen, T., Moeder, M., Arukwe, A., 2010. Municipal landfill leachates: A significant source for new and emerging pollutants. *Sci. Total Environ.* 408, 5147-5157.
3. Renou, S., Givaudan, J.G., Poulain, S., Dirassouyan, F., Moulin, P., 2008. Landfill leachate treatment: Review and opportunity. *J. Hazard. Mater.* 150, 468-493.
4. Abbas, A.A., Jingsong, G., Ping, L.Z., Ya, P.Y., Al-Rebaki, W.S., 2009. Review on Landfill Leachate Treatments. *J. Appl. Sci. Res.* 5, 534-545.
5. De Moraes, J.L., Zamora, P.P., 2005. Use of advanced oxidation processes to improve the biodegradability of mature landfill leachates. *J. Hazard. Mater.* 123, 181-186.
6. Deng, Y., Englehardt, J.D., 2007. Electrochemical oxidation for landfill leachate treatment. *Waste Manage.* 27, 380-388.
7. Anglada, A., Urtiaga, A., Ortiz, I., Mantzavinos, D., Diamadopoulos, E., 2011. Boron-doped diamond anodic treatment of landfill leachate: Evaluation of operating variables and formation of oxidation by-products. *Water Res.* 45, 828-838.
8. Fernandes, A., Pacheco, M.J., Ciriaco, L., Lopes, A., 2012. Anodic oxidation of a biologically treated leachate on a boron-doped anode. *J. Haz. Mat.* 199-200, 82-87.
9. Panizza, M., Cerisola, G., 2009. Direct and mediated anodic oxidation of organic pollutants. *Chem. Rev.* 109, 6541-6569.
10. Eaton, A., Clesceri, L., Rice, E., Greenberg, A., Franson, M.A., 2005. *Standard Methods for Examination of Water and Wastewater*, twenty-first ed.. American Public Health Association, Washington, DC.

Acknowledgements

Financial support from FEDER, Programa Operacional Factores de Competitividade – COMPETE, and FCT, for the projects PTDC/AAC- AMB/103112/2008 and PEst-OE/CTM/UI0195/2011 of the MT&P Unit and for the grant awarded to A. Fernandes SFRH/BD/81368/2011.

Photocatalytic degradation of Rhodamine 6G by nanocrystalline $\text{Ca}_{0.6}\text{Ho}_{0.4}\text{MnO}_3$ film under visible light

B. Barrocas¹, A. Rovisco², Y. Nunes², S. Sérgio², M.E. Melo Jorge¹

¹CCMM, Departamento de Química e Bioquímica, Faculdade de Ciências da Universidade de Lisboa, Campo Grande, 1749-016 Lisboa, Portugal, ²CEFITEC, Departamento de Física, Faculdade de Ciências e Tecnologia da Universidade Nova de Lisboa, 2829-516 Caparica, Portugal.

Abstract

In this work, the perovskite ($\text{Ca}_{0.6}\text{Ho}_{0.4}\text{MnO}_3$) film was prepared by RF-magnetron sputtering from nanosized powder target previously prepared by self-combustion method using citric acid and the catalytic activity was examined on the decolorization of Rhodamine 6G (Rh6G) aqueous solutions. The $\text{Ca}_{0.6}\text{Ho}_{0.4}\text{MnO}_3$ film showed a promising photocatalytic performance under visible light irradiation, with very low variation of decay rate after two consecutive usages. The structural and morphological characterization was performed by XRD and DRIFTS, and revealed high stability of the film after two successive photodegradations assays.

Introduction

Textile and industrial dyes are a major source of water contamination and therefore, many methods have been used for the purification of water contaminated with dyes [1]. The most efficient method for water purification, destroying organic pollutants is heterogeneous photocatalysis [2].

Many materials have been studied and tested for use as catalysts in photodegradation studies, such as TiO_2 , CdS, WO_3 and others, but the TiO_2 is one of the most studied semiconductors for photocatalytic reactions because it shows a high reactivity under ultraviolet (UV) light and it is nontoxic, stable and inert chemically. However, TiO_2 only becomes active under irradiation with ultraviolet UV light whose energy exceeds the band gap of 3.2 eV in the anatase crystalline phase. This inhibits the utilization of solar light as a sustainable energy source for TiO_2 activation because only 5 % of the incoming solar energy on the earth's surface is in the UV range [3-5]. In this context, it is important to search other alternative materials that can have a photoresponse in the visible range. Ternary metal oxides with different crystal structures show excellent photoactivity due to the orientation of atoms in a layer structure and the presence of vacancies in the crystal structure. For example, different crystal structures such as perovskites (ABO_3), pyrochlores ($\text{A}_2\text{B}_2\text{O}_7$), spinels (AB_2O_4), and delafossites (ABO_2) are of interest as photocatalysts [6]. Therefore, perovskites are a family of interesting compounds that can offer the desired properties for an ideal photocatalyst. Recently, perovskites have been explored as potential materials for photocatalytic applications. Compounds like

LaNiO_3 , CeAlO_3 [1], CeVO_3 , PrVO_3 , NdVO_3 [7], SrFeO_3 [8], SrTiO_3 , NaTaO_3 , NaNbO_3 , KNbO_3 and KTaO_3 [9] have been reported to have p-type semiconductor characteristics and, for that reason, they are photocatalytically active using UV and visible light [10]. The band structure of the perovskites has been reported to be responsible for making the perovskites photocatalytically active [11]. Therefore, it is desirable to explore the photocatalytic properties of perovskites [1, 12]. The general formula of manganite perovskite-type structure is $\text{A}_{1-x}\text{Ln}_x\text{MnO}_3$ (A = alkaline earth, Ln = rare earth) [13]. In this work the $\text{Ca}_{0.6}\text{Ho}_{0.4}\text{MnO}_3$ catalyst was prepared with perovskite structure, by RF-magnetron sputtering using nanosized powder target. This work reports also some preliminary results of the photodegradation under visible light of Rh6G using the $\text{Ca}_{0.6}\text{Ho}_{0.4}\text{MnO}_3$ film.

Materials and Methods

$\text{Ca}_{0.6}\text{Ho}_{0.4}\text{MnO}_3$ film was deposited at room temperature by RF-magnetron sputtering from a nanosized powder target previously prepared by self-combustion method using citric acid, as described in detail in previous works [15, 16]. The sputtering target was prepared by mixing the synthesized powder with acetone. The mixture was placed on the cathode top and it was pressed and compacted until the acetone evaporation. The target was sputtered in 99.999% pure argon at constant total sputtering gas pressure (P_{Tot}) of 0.23 Pa and the deposition time was 80 min. It was used a RF power supply: Plasmaloc 2HF and the deposition was done using a sputtering power of 25 W and frequency = 100 KHz. The manganite film was deposited on an unheated fused silica substrate. In order to allow the crystalline growth, the film was annealed at 800 °C in air during 6 h.

The structural characterization of the film was carried out by X-ray diffraction (XRD) on a Philips Analytical PW 3050/60 X'Pert PRO (theta/2 theta) equipped with X'Celerator detector and with automatic data acquisition (X'Pert Data Collector (v2.0b) software), using a monochromatized $\text{CuK}\alpha$ radiation as incident beam, 40 kV–30 mA. Diffractograms were obtained by continuous scanning in a 2θ -range of 10° to 90° with a 2θ -step size of 0.02° and a scan step time of 20 s.

The surface morphology and thickness of the film was examined by field-emission scanning electron microscope (FEG-SEM JEOL 7001F). In order to prevent charge

build up a thin gold film was coated on the film during analysis.

For a detailed study of the surface, an atomic force microscope (AFM) was used, AFM Topometrix TMX 2000 (Veeco Instruments), in contact mode. Silicon cantilevers were employed. The images were taken with 400×400 pixels resolution and with an area of 1×1 μm². A one step-leveling was applied to the images for accurate measurement of Z-height across a sample without adding any erroneous tilt information to the data and the root mean square roughness (Rrms) was calculated by Topometrix software.

All the photodegradation experiments were conducted using a 250 mL refrigerated photoreactor [2]. The radiation source used was a 450 W Hanovia medium-pressure mercury-vapour lamp, the total irradiated energy being 40-48% in the ultraviolet range and 40-43% in the visible region of the electromagnetic spectrum. A glass filter was used in order to eliminate the UV radiation. The catalytic photodegradation assays were performed using Ca_{0.6}Ho_{0.4}MnO₃ film with geometric area (9.75 cm²) into 175 mL of 5 ppm Rh6G aqueous solution. Prior to irradiation, the solutions were stirred in darkness for 1 h to ensure the adsorption equilibrium. During irradiation, with visible light, the solutions were sampled at regular intervals and analyzed by UV-vis spectroscopy. A UV-vis spectrophotometer Shimadzu UV-2600 was used for monitoring the absorption of the Rh6G solutions and the rate of decolorization was observed in terms of change in intensity at λ_{max} of the dye (526 nm). The decolorization photocatalytic efficiency (%) has been calculated as:

$$\text{Photocatalytic Efficiency (\%)} = \frac{C_0 - C}{C_0} \times 100$$

where C_0 is the initial concentration of dye and C is the concentration of dye after photoirradiation. In order to study the reusability of the catalysts, all the experimental parameters were kept constant and the experiments were repeated for 2 sets using the same catalyst and fresh dye solutions. After each photodegradation assay the catalyst was cleaned with distilled water to remove any organic contamination. The films structural stability was also checked after each photodegradation assay by XRD. The surface of the catalyst was studied using diffuse reflectance infrared Fourier transform spectroscopy (DRIFTS) before de photocatalytic assays and after each reuse.

The diffuse reflectance infrared Fourier transform spectra (DRIFTS) were obtained on a Nicolet 6700 FT-IR attached to Smart Diffuse Reflectance Accessory, in the region 400-4000 cm⁻¹. The background was done using a gold plate and the data acquisition was performed using the program Omnic.

Results and Discussion

The XRD pattern for the annealed manganite film depicted in figure 1, revealed the formation of perovskite-

type phase with orthorhombic symmetry, space group *Pnma*.

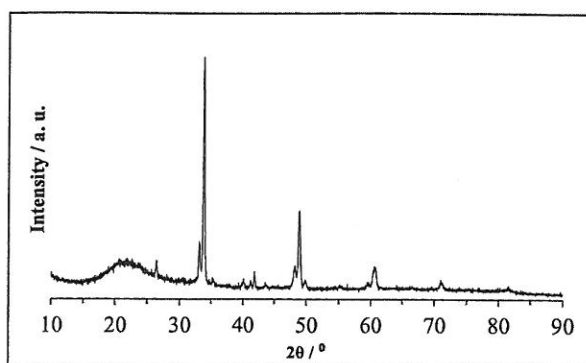
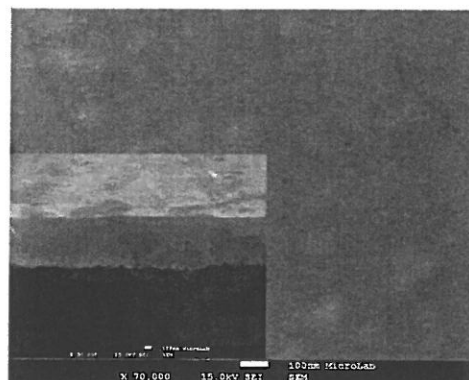


Figure 1 - XRD patterns of the annealed manganite (Ca_{0.6}Ho_{0.4}MnO₃) film deposited in fused silica substrate.

The surface morphology of the Ca_{0.6}Ho_{0.4}MnO₃ film was analyzed with SEM and AFM techniques (Figure 2). Both techniques show a film with a smooth and homogeneous surface texture, with a surface roughness of approximately 1.09 nm. The film presents a thickness of 890 nm.

a)



b)

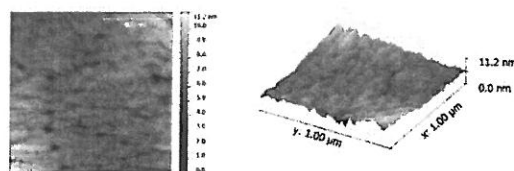


Figure 2 - a) SEM images (surface and cross-sectional image) b) AFM images (two- and three-dimensional images) of the Ca_{0.6}Ho_{0.4}MnO₃ film.

To study the catalytic activity, the film was tested in the photodegradation of an organic dye, Rh6G. For comparative purposes the Rh6G photolysis (without any catalyst) was also performed.

Figure 3 shows typical time dependent UV-vis spectra of Rh6G decolorization with annealed $\text{Ca}_{0.6}\text{Ho}_{0.4}\text{MnO}_3$ film catalyst during 8 hours of visible light irradiation.

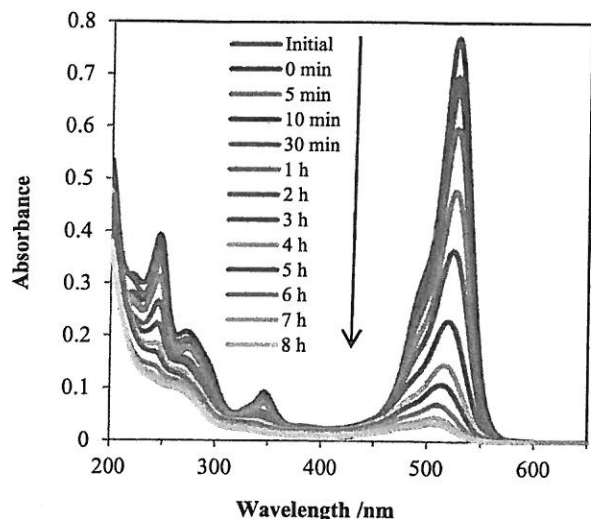


Figure 3 - Absorbance spectra of Rh6G solution during the first photodegradation experiment, using the $\text{Ca}_{0.6}\text{Ho}_{0.4}\text{MnO}_3$ film as catalyst.

Rh6G presents the main absorption peaks at 526 nm in visible region and 276 and 343 nm in UV region. The rate of decolorization was recorded with respect to the change in intensity of absorption peak at 526 nm. During the 8 hours of irradiation this absorption peak diminished, indicating that the dye has been degraded.

Using the data from the UV-vis spectra obtained after each degradation was possible to represent graphically the photodegradation curves of 175 mL aqueous solution of 5 ppm Rh6G over time. The obtained results are present in Figure 4.

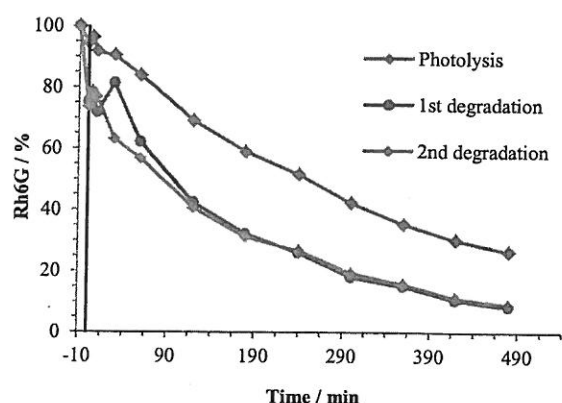


Figure 4 - Rh6G degradation percentage evolution during the several photocatalytic degradations of a 5 ppm aqueous solution for the $\text{Ca}_{0.6}\text{Ho}_{0.4}\text{MnO}_3$ film.

As can be seen from Figure 4 the material tested demonstrated to be catalytic in this photodegradation process. After 8 hours of irradiation with visible light no significantly Rh6G was detected in the solution. It can be observed that the $\text{Ca}_{0.6}\text{Ho}_{0.4}\text{MnO}_3$ film, when used for the first time, could degrade 91.5% dye, with a very small change to 90.9% in the efficiency when used for second time. This result reveals that $\text{Ca}_{0.6}\text{Ho}_{0.4}\text{MnO}_3$ film to be good dye-decolorizing using visible light and a promising catalytic after two consecutive usages.

To evaluate the film photochemical stability after successive photodegradations assays it was performed the structural characterization by XRD and DRIFT spectra, after each degradation and the obtained results are depicted in Figures 5 and 6, respectively. The XRD data of the reused $\text{Ca}_{0.6}\text{Ho}_{0.4}\text{MnO}_3$ film shows that there were no additional phases and the data matched with the fresh $\text{Ca}_{0.6}\text{Ho}_{0.4}\text{MnO}_3$. This indicated that $\text{Ca}_{0.6}\text{Ho}_{0.4}\text{MnO}_3$ film did not leach out/corrode after reusing it in two consecutive assays. It can also be observed that the crystalline structure of the film remains the same after the successive degradations. The DRIFTS data of the reused $\text{Ca}_{0.6}\text{Ho}_{0.4}\text{MnO}_3$ film shows the absence of any organic species on the film surface.

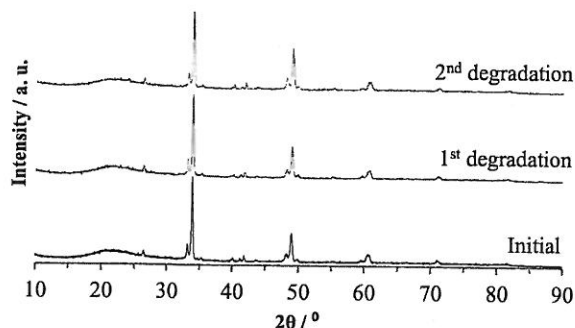


Figure 5 - XRD patterns of the $\text{Ca}_{0.6}\text{Ho}_{0.4}\text{MnO}_3$ film after each photodegradation experiment.

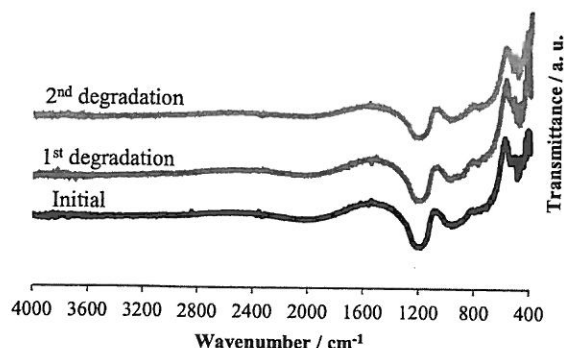


Figure 6 - DRIFTS spectra of the $\text{Ca}_{0.6}\text{Ho}_{0.4}\text{MnO}_3$ film after each photodegradation experiment.

Therefore, the reuse of the $\text{Ca}_{0.6}\text{Ho}_{0.4}\text{MnO}_3$ film show a promising performance not only in the stability but also with very low variation of decay rate after two consecutive usages.

Conclusions

The reuse of $\text{Ca}_{0.6}\text{Ho}_{0.4}\text{MnO}_3$ manganite film prepared by magnetron sputtering technique using nanosized powder compacted target was evaluated in the degradation of Rh6G. Under visible light irradiation the $\text{Ca}_{0.6}\text{Ho}_{0.4}\text{MnO}_3$ film has worked efficiently to degrade Rh6G in aqueous phase. The film show a promising catalytic performance without significant decrease in the removal efficiency after two consecutive usages. XRD revealed high stability of the films after successive photodegradations assays and DRIFTS revealed that the film has no adsorbed organic species on the surface.

References

1. Deshpande, P., Aruna, S., Mandas, G., Clean - Soil, Air, Water, 39, 259, 2011.
2. Franco, A., Neves, M., Ribeiro Carrott, M., Mendonça, M. H., Pereira, M. I., Monteiro, O. C., J. Hazard. Mater., 161, 545, 2009.
3. Zhao, S., Li, J., Wang, L., Wang, X., Clean - Soil, Air, Water, 38, 268, 2010.
4. Chen, P., Zhang, X., Clean - Soil, Air, Water, 36, 507, 2008.
5. Bhatkhande, D., Pangerkar, V., Beenackers, A., J. Chem. Technol. Biotechnol., 77, 102, 2001.
6. Murugesan, S., Huda, M., Yan, Y., Al-Jassim, M., Subramanian, V., J. Phys. Chem. C, 114, 10598, 2010.
7. Saha, D., Mahapatra, S., Row, T., Madras, G., Ind. Eng. Chem. Res., 48, 7489, 2009.
8. Yang, Y., Cao, Z., Jiang, Y., Liu, L., Sun, Y., Mater. Sci. Eng., B, 132, 311, 2006.
9. Huang, Y., Xie, Y., Fan, L., Li, Y., Wei, Y., Lin, J., Wu, J., Int. J. Hydrogen Energy, 33, 6432, 2008.
10. Li, Y., Yao, S., Wen, W., Xue, Z., Yan, Y., J. Alloys Compd., 491, 560, 2010.
11. Kim, T., Hur, S., Hwang, S., Park, H., Park, Y., Choi, W., Choy, J-H., Mater. Res. Bull, 42, 1914, 2007.
12. Deshpande, P., Madras, G., Chem. Eng. J., 158, 571, 2010.
13. Ferreira, B. M., Melo Jorge, M. E., Lopes, M. E., Nunes, M.R., Silva Pereira, M.I., Electrochimic. Acta, 54, 5902, 2009.
14. Sérgio, S., Melo Jorge, M. E., Maneira, M. J. P., Nunes, Y., Mat. Chem. Phys., 126, 73, 2011.
15. Sousa, D., Nunes, M. R., Silveira, C., Matos, I., Lopes, A. B., Melo Jorge, M. E., Mater. Chem. Phys., 109, 311, 2008.
16. Isasi, P. H., Lopes, M. E., Nunes, M. R., Melo Jorge, M. E., J. Phys. Chem. Solids, 70, 405, 2008.

Acknowledgements

Financial support from FEDER, through Programa Operacional Factores de Competitividade – COMPETE, and Fundação para a Ciência e a Tecnologia – FCT, for the project PTDC/AAC-AMB/103112/2008.

The authors acknowledge the financial support FCT, for the projects PEst-OE/FIS/UI0068/2011 and PEst-OE/QUI/UI0536/201. S. Sérgio for the Programme Ciência 2007.

Environmental applications of TiO₂ electrodes prepared by DC-Magnetron Sputtering

S. Ferreira¹, S. Sérgio², M.E. Melo Jorge³, L. Ciriaco¹, M. J. Pacheco¹, A. Lopes¹

¹ Departamento de Química, UIMP, Universidade da Beira Interior, 6201-001 Covilhã, Portugal

² CEFITEC, Dep. Física, Faculdade de Ciências e Tecnologia da Universidade Nova de Lisboa, 2829-516 Caparica, Portugal

³ CCMM, Departamento de Química e Bioquímica, Faculdade de Ciências da Universidade de Lisboa, Lisboa, Portugal,

Abstract

The objective of this work was to assess the potential of TiO₂ catalytic films, prepared by DC-magnetron sputtering, in the degradation of Acid Orange 7 (AO7) aqueous solutions using heterogeneous photo-catalysis or photoelectrocatalysis. Photolysis assays were also run. The assays were conducted in a system operating in batch mode, with stirring, for 4 hours, using a thermostatic bath to maintain constant the temperature (25 °C). Two UV lamps of 7 W each were used in the photocatalytic assays. In the electrolytic experiments, TiO₂ films, deposited on a conductive glass (F-doped tin oxide (SnO₂:F)), FTO substrate, or the just the FTO substrate, were used as anode and stainless steel as cathode. The applied current was 1 mA cm⁻². In all the experiments, the initial concentration of dye was 50 ppm. The samples were analyzed for chemical oxygen demand (COD) and total organic carbon (TOC) content. Spectrophotometry UV-Vis absorption spectra were also carried out. COD removals varied between 3% and 44% and TOC removals were always lower. These low removals actually contradict the removals in absorbance obtained from the absorption spectra, making it clear that the degradation mechanism is mainly by conversion of the dye molecule than by its mineralization. Spectrophotometric studies showed an effective AO7 removal ranging between 15 and 44 ppm.

Although the good results that were obtained in this preliminary study, the catalytic effect of TiO₂ in the assays involving catalytic processes have indicated that in the experimental conditions tested the TiO₂ did not have the desired effect.

Introduction

The industrial development and the increase in population are causing an accumulation of persistent pollutants that degrade the environment and attacks ecosystems. Dyes and other aromatic compounds are among those responsible for this problem and it became necessary to develop processes that are able to stop this disaster. Although the biological methods are the cheapest way to reduce pollution in the liquid effluents, they are not always effective and has become imperative the development of new and more active methods, like photoelectrocatalytic methods. They are advantageous beyond doubt and photocatalysis is being intensively study due to its high efficiency in the removal of color from dye baths [1,2,3,4].

The degradation mechanism of the polluting compounds by photocatalysis is illustrated in Figure 1.

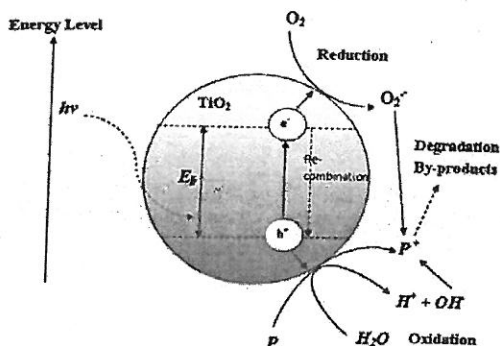
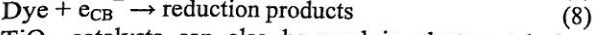
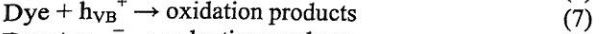
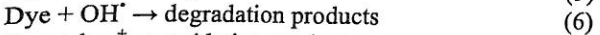
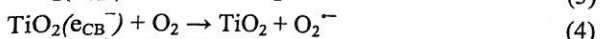
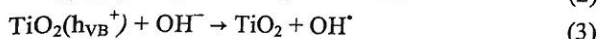
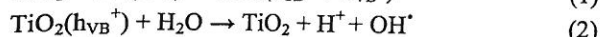
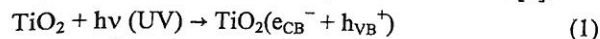


Figure 1 - Mechanism of the formation of the pair electron-hole in a TiO₂ semiconductor in the presence of a pollutant molecule P (adapted from [5]).

Conduction band electrons (e_{CB}^-) and valence band holes (h_{VB}^+) are generated when TiO₂ film is irradiated with light energy higher than its band gap energy (E_g , 3.2 eV). The photogenerated electrons could reduce the dye (pollutant molecule) or react with electron acceptors such as O₂ adsorbed on the Ti(III)-surface or dissolved in water, reducing it to superoxide radical anion O₂⁻. The photogenerated holes can oxidize the organic molecule or react with OH⁻ or H₂O oxidizing them into OH[·] radicals. Together with other highly oxidant species (peroxide radicals) they are reported to be responsible for the heterogeneous TiO₂ photodecomposition of organic compounds such as dyes. According to this, the relevant reactions at the semiconductor surface causing the degradation of dyes can be expressed as follows [1]:



TiO₂ catalysts can also be used in electrocatalysis or photoelectrocatalysis as anode. Figure 2 presents the mechanism of the electrodegradation at the anode of the organic molecule R mediated by OH[·]. The degradation can take place via combustion or conversion. In the latter

case, if the resulting by-products are biodegradable, it may correspond to a successful process.

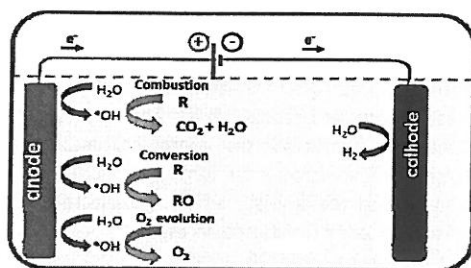


Figure 2 - Mechanism of the anodic oxidation of the organic molecule R, mediated by OH^\bullet .

Materials and Methods

The TiO_2 films used in the degradation assays were deposited by DC reactive magnetron sputtering on conductive glass (F-doped tin oxide ($\text{SnO}_2:\text{F}$)) substrates (FTO substrates) at room temperature in a custom made system as previously reported and described in detail elsewhere [6]. A titanium disc (99.99% purity) having 64.5 mm of diameter and 4 mm of thickness was used as sputtering target. The gases in the system were 99.99% pure Ar and O_2 , and partial pressures of these gases were separately controlled by mass flow controllers. The total pressure, P_T , during the deposition was kept constant at 0.8 Pa and the partial pressure of oxygen was 0.8 Pa (i.e. 10% of P_T). The sputtering power was kept at 1000 W and the deposition time was 80 min. In order to improve crystalline growth the as-sputtered films were thermal annealed in air at 400 °C for 4 h in a tubular furnace.

The structural characterization was carried out on a Philips Analytical PW 3050/60 X'Pert PRO ($\theta/2\theta$) equipped with X'Celerator detector and with automatic data acquisition (X'Pert Data Collector (v2.0b) software), using a monochromatized Cu $K\alpha$ radiation as incident beam, 40 kV–30 mA. Diffractograms were obtained by continuous scanning in a 2θ -range of 20–90° with a scan step time of 20 s. For the degradation assays, two 7 W UV lamps (254 nm) were deepened in the solution, with the TiO_2 film (5 cm^2 geometric area) between.

The electrocatalytic experiments were conducted using a Potentiostat/Galvanostat, VoltaLab PGZ 301, as power source, being the applied current density 1 mA cm^{-2} . The assays were performed in a three electrodes cell, of one compartment, being the anode the FTO/ TiO_2 film or just the substrate (FTO), the cathode a stainless steel foil and the reference electrode a commercial Ag/AgCl, KCl sat. As model solution, 170 mL of an aqueous AO7 50 ppm solution in 5 g L^{-1} Na_2SO_4 was used.

Before starting the test, the solution, with the electrodes immersed, was stirred for one hour. After that, a sample was collected from the solution and analyzed by UV-Vis spectrophotometry, to exclude the hypothesis of dye adsorption on the surface of the electrodes. The assay was then started and run during 4 h.

The samples collected during the assays were analysed, according to standard procedures for the following parameters: Chemical oxygen demand, using closed reflux dichromate titrimetric method; Total organic carbon (TOC), measured using a TOC analyser, Shimadzu TOC-V CPH; UV-Visible absorption spectrophotometric analyses, with absorbance (Abs) measurements from 200 to 800 nm, using a Shimadzu UV-1800 spectrophotometer.

Results and Discussion

Figure 3 shows the XRD diffraction pattern obtained for the heated FTO/ TiO_2 film. It can be observed a small diffraction peak with (101) orientation at 2θ near to 25° typical of the anatase TiO_2 structure (JCPDS/ICDD 21-1272). The average crystallite size for the TiO_2 film was calculated from the broadening of this diffraction peak using the Scherrer's formula, $D = 0.9\lambda/B \cos\theta$, where λ is the wavelength of Cu $K\alpha$ radiation, B is the full width at half maximum (FWHM) of XRD peaks and θ the Bragg diffraction angle of the line. A value of ~60 nm for the anatase TiO_2 crystallite size was estimated. All the other reflections correspond to the FTO substrate.

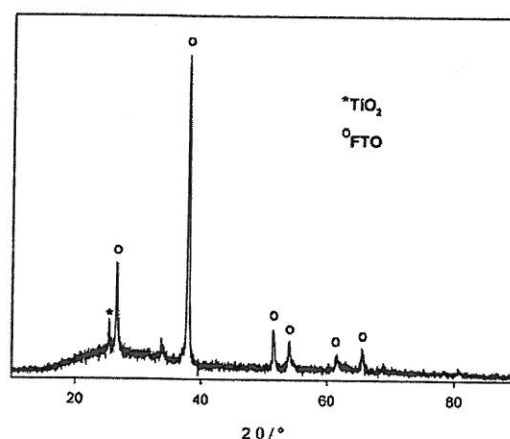


Figure 3. XRD diffraction pattern of TiO_2 deposited on FTO substrate.

Table 1 presents the removals in COD, TOC and AO7 concentration, determined by UV-Vis spectrophotometry at 485 nm, for the different assays performed, with the FTO and with FTO/ TiO_2 film. The variation in time of absorbance, measured at 485 nm, for those assays is depicted in Figure 4.

COD removals in the assays performed with FTO/ TiO_2 film are higher than those obtained in the assays performed with the substrate alone. However, the best COD removal was obtained in the photolysis assay, which signifies that the most effective process for the degradation of AO7 is the UV light, and the presence of the substrate or substrate+ TiO_2 film only prevents light to reach the solution. TOC removals are negligible and COD and color removals are similar, meaning that the

degradation of the dye happens mainly by a conversion mechanism.

In Figure 5, the spectra for the samples collected during some of the performed assays are presented. There is a regular decay in time of the absorbances in the visible region. On the other hand, at UV wavelengths these decay is not so regular and, in some cases, there is an increase in the absorbances measured in the region 200-300 nm, which may be due to the break of the azo bond, with the consequent increase in the aromatics concentration, that absorb in that region of the spectrum.

Table 1. Removals of the monitored parameters after 4 h assay. AO7 concentration determined by UV-Vis at 485 nm.

| Processes | Removal | | |
|---|---------------------|-------|-------|
| | Δ AO7* / ppm | % COD | % TOC |
| Photolysis | 41 | 44 | 3 |
| Photocatalysis (substrate) | 15 | 3 | 3 |
| Electrocatalysis (substrate) | 36 | 3 | 0 |
| Photoelectrocatalysis (substrate) | 37 | 38 | 3 |
| Photocatalysis (TiO ₂) | 24 | 32 | 0 |
| Electrocatalysis (TiO ₂) | 24 | 5 | 0 |
| Photoelectrocatalysis (TiO ₂) | 44 | 41 | 0 |

*Variation of AO7 concentration during the assay.

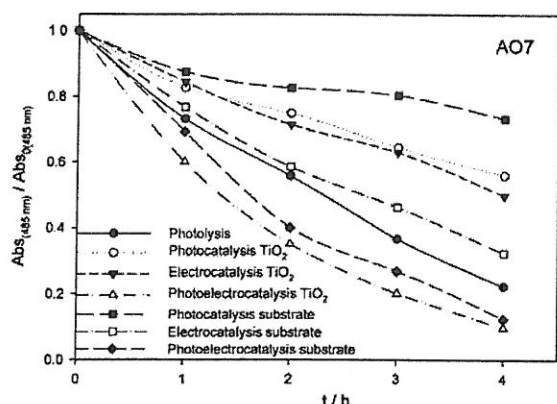


Figure 4 – Variation with time of the absorbance, measured at 485 nm, for the different assays performed.

Conclusions

From the degradation study of AO7 with TiO₂ films, performed with different techniques, the following conclusions can be drawn:

- In general, AO7 degradation is possible using TiO₂ films, either by photocatalysis, electrocatalysis or photoelectrocatalysis, since AO7 removals between 15 and 44 ppm were observed only after 4 h degradation.
- Good color removal was detected by UV-Vis spectrophotometry, being, however, COD removals lower and TOC removals almost inexistent.

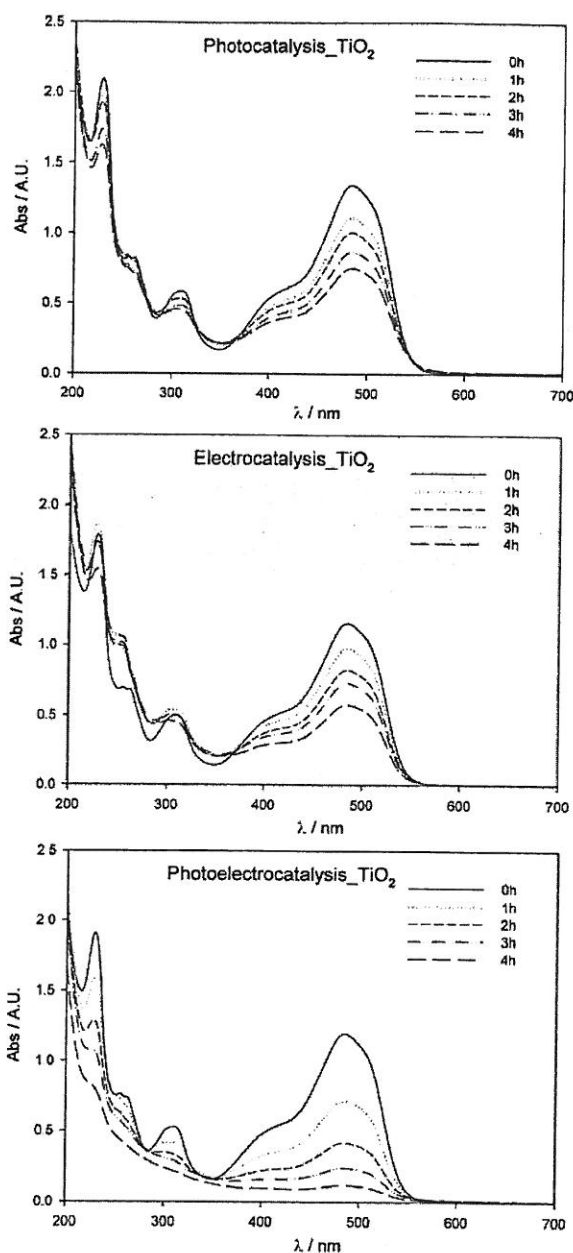


Figure 5 – UV/Vis spectra for the assay of photoelectrolysis with TiO₂ film

- TiO₂ films have not enough stability when current density is higher than 1 mA cm⁻².
- After 4 h assay, the absorbance removal at 485 nm was almost complete in photoelectrolysis process, being lower for all the others processes.
- Photolysis presents better results than TiO₂ photocatalysis, probably because the most influent factor is the UV light that is prevented from reaching the solution due to the presence of the film.

References

1. Ioannis K. Konstantinou, Triantafyllos A. Albanis, 2004. TiO₂-assisted photocatalytic degradation of azo dyes in aqueous solution: kinetic and mechanistic investigations: A review, *Appl. Catal. B-Environ.* 49, 1-14.
2. Akpan U.G., Hameed B.H., 2009. Parameters affecting the photocatalytic degradation of dyes using TiO₂-based photocatalysts: A review, *J. Hazard. Mater.* 170, 520-529.
3. Soutsas K., Karayannis V., Poullos I., Riga A., Ntampeglitis K., Spiliotis X., Papapolymerou G., 2010. Decolorization and degradation of reactive azo dyes via heterogeneous photocatalytic processes, *Desalination* 250, 345-350.
4. Barrocas, B., Monteiro, O.C., Melo Jorge, M.E., Sérgio, S. 2013. Photocatalytic activity and reusability study of nanocrystalline TiO₂ films prepared by sputtering technique, *Appl. Surf. Sci.*, 264, 111-116.
5. Chong, M., Jin, B., Chow, C., Saint, C. 2010. Recent developments in photocatalytic water treatment technology: A review. *Water Res.* 44, 2997-3027.
6. Sérgio, S. Melo Jorge, M.E., Maneira, M.J.P., Nunes, Y. 2011. Influence of O₂ partial pressure on the growth of nanostructured anatase phase TiO₂ thin films prepared by DC reactive magnetron sputtering, *Mat. Chem. Phys.*, 126, 73-81.

Acknowledgements

Financial support from FEDER, Programa Operacional Factores de Competitividade – COMPETE, and FCT, for the projects PTDC/AAC- AMB/103112/2008 and PEst-OE/CTM/UI0195/2011 of the MT&P Unit

Heavy metals monitoring during the electrochemical treatment of municipal landfill leachates

A. D. Fonseca, P. Spranger, A. Fernandes, L. Ciriaco, A. Lopes, M.J. Pacheco
UMTP and Department of Chemistry, University of Beira Interior, 6201-001 Covilhã, Portugal

Abstract

The aim of this study is to evaluate the removal of heavy metals (Fe, Zn and Cr) during an electrochemical combined treatment, electrocoagulation (EC), using a consumable iron anode, followed by anodic oxidation (AO) with a BDD anode, of a landfill leachate samples, collected in a municipal landfill in the Beira Interior region. In EC experiments, it was observed an iron content fluctuation, mainly due to the cycles of iron hydroxyl formation and precipitation. During AO, the iron removal was 85%. After EC, zinc and chromium content removals were about 65%. After the combined treatment, removals were almost complete.

Introduction

Solid wastes containing heavy metals and other species can be a serious environmental problem. Once released to the environment, these species may accumulate in soils in different forms, as water-soluble extractable compounds or linked to carbonates, iron-manganese oxides and organic matter. The species in the solid waste that are soluble and extractable in water are considered bioavailable and are likely to be transported to the water and, as a consequence, can be absorbed by plants and can eventually bioaccumulate in the food chain [1]. In some cases, these solid wastes containing heavy metals are disposed in municipal sanitary landfills. The heavy metals can remain trapped in the landfills and eventually be released to the environment, due to generation of leachates caused by the rainwater percolation through the solid wastes and wastes decomposition [2]. In fact, compared to the total amount of heavy metals disposed into landfills the content of heavy metals in leachate is relatively low. The major part of the metals is retained in the landfill. As a consequence, it must be expected that leaching of heavy metals from the landfills will continue for a long time [3].

Besides heavy metals, leachates also contain various pollutants such as organic matter, biodegradable and non-biodegradable, ammonia-nitrogen, chlorinated organic and inorganic salts [4]. Some of these pollutants can be removed by biological treatment but heavy metals and non-biodegradable organic matter are bio-refractory.

So, the leachate treatments to reduce high contents in organic matter and simultaneously heavy metals contents represent a big challenge. Thus, a combined treatment approach may be the solution to minimize the environmental impact of these complex wastewaters. In this context, several studies have proved the feasibility of electrochemical technologies, namely electrocoagulation (EC) and anodic oxidation (AO), for the treatment of landfill leachates [5,6].

The objective of this study is to evaluate the removal of heavy metals (Fe, Zn and Cr) during a combined treatment, EC followed by AO, of leachates coming from a municipal landfill in the Beira Interior region.

Materials and Methods

Sample collection

The leachate samples were provided by a Beira Interior municipal sanitary landfill.

The samples were collected in containers of 25 L, just before the biological treatment. In the laboratory, the samples were stored at 4°C until processing and analysis.

Electrochemical Experiments

Electrocoagulation experiments were conducted in batch mode, without stirring and using 500 mL of leachate. Iron electrodes were used as cathode and as anode, both with an immersed area of 40 cm², with a 1.0 cm gap between them. All experiments were conducted with an applied current intensity of 2.5 A, at room temperature and without addition of background electrolyte, during three hours. After the EC treatment, the samples were allowed to settle and the supernatant liquid was then submitted to the anodic oxidation treatment. Anodic oxidation experiments were conducted in batch mode, with stirring, and using 200 mL of the electrocoagulated effluent, during eight hours. A BDD anode, with an immersed area of 20 cm², and a stainless steel cathode, with identical area, were used. Different current intensities were applied, namely, 1.0 and 1.4 A. During both electrochemical experiments,

samples were withdrawn at various time intervals and analyzed for the total Fe, Zn and Cr content.

Analyses

The samples withdrawn during EC were centrifuged and 10 mL of the supernatant solution was submitted to an HCl-HNO₃ acid digestion according to a procedure described in the Standard Methods for the Examination of Water and Wastewaters [7]. The AO samples were submitted to the same treatment without the centrifugation step.

The total Fe, Zn and Cr contents were determined by Flame Atomic Absorption Spectrometry, using a SP9 Pye Unicam apparatus.

All glassware used in the analyses had been pre-cleaned and acid-washed before use. All reagents were of analytical grade and were used without further purification.

All tests were repeated at least twice, to guarantee the reproducibility of the results.

Results and Discussion

During EC, the iron consumable anode oxidizes and iron ions are formed. In solution, these ions hydrolyze and, depending on the medium pH, different polymeric hydroxides may be formed. These polymeric hydroxides are excellent coagulation agents, which have strong affinity for colloids, dispersed particles and ionic species forming flocs that can be removed by sedimentation and/or flotation [8]. In the present study, in order to understand the iron behavior during the EC treatment, the variation of iron in the solution was monitored and results are presented in Figure 1.

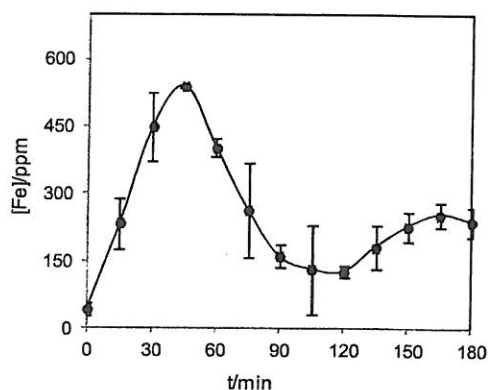


Figure 1 – Evolution of dissolved iron during EC treatment, performed at applied current intensity of 2.5 A, during 3 h.

In the first 45 min of the EC treatment, the dissolved iron content in the wastewater increased sharply, due to the oxidation of the iron consumable anode that generates Fe²⁺ in solution, followed by a fall, due to the growth of polymeric iron hydroxyl flocs, which were transformed in non soluble forms. The iron content fluctuation during EC treatment is mainly due to these cycles of iron hydroxyl formation and precipitation.

Figure 2 presents the total Fe, Zn and Cr contents before and after three hours of EC treatment and after the combined treatment, three hours of EC followed by eight hours of AO.

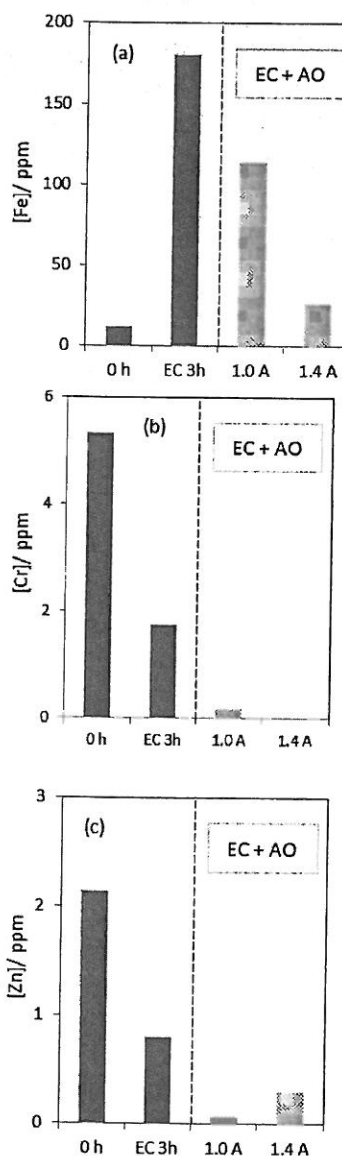


Figure 2- Heavy metal concentration before and after EC and after the combined treatment EC (3 h) + AO (8h): (a) iron; (b) chromium; (c) zinc.

As it was expected, for the reasons mentioned previously, in the end of the EC treatment, the iron content value is higher than the initial value (Fig. 2 a). During the anodic oxidation performed with the highest current intensity, 85% of the iron was removed.

Regarding the total of chromium and zinc concentrations at the end of the EC and the combined treatment (Fig. 2 b and c), they have decreased during both processes. After the EC, the zinc and chromium removals were 63% and 67%, respectively. In the final of the combined treatment, for the AO performed at the applied current intensity of 1.4 A, the chromium removal was almost complete, its concentration was lower than the limit of detection of the method. In the case of zinc, the best removal, 96%, was obtained for the applied current intensity of 1,0 A.

Heavy metals removal by these two combined electrochemical methods may involve two processes: in the EC, the co-precipitation with the formed iron hydroxyl polymeric flocs and, simultaneously, the reduction in the cathode, with the correspondent deposition on it, and in AO mainly due to the latter process.

Conclusions

During electrocoagulation there is an increase in the iron content, mainly due to the oxidation of the iron consumable anode. The iron content fluctuation during EC is mainly due to the cycles of iron hydroxyl formation/precipitation. During AO, 85% of the iron formed during EC, which remains in the EC treated effluent, is removed and the removal efficiency increases with applied current density. At the end of the combined treatment, the chromium and zinc are almost completely removed; the legal limits for disposal into the municipal sewage were accomplished.

References

- [1] T.A. Maranhão, J.S.A. Silva, R.M. Andrade, V.L.A.F., Bascuñan, F.J.S Oliveira, A.J. Curtius. Determination of As and Hg in acetic extract by vapor generation coupled to atomic spectrometry for solid waste classification. *Microchem. J.* 106 (2013) 139-146.
- [2] M. Aucott. The Fate of Heavy Metals in Landfills. *TheTidal Exchange* 21 (2008) 1-5.
- [3] Heavy Metals in Waste-Final report. E3 Project ENV.E.3/ETU/2000/0058. European Commission DG ENV (2002).

- [4] Z.P. Wang, Z. Zhang and Y.J. Lin Landfill leachate treatment by coagulation-photooxidation process. *J. Hazard. Mat.* 95 (2002) 153-159.
- [5] A. Fernandes, M.J. Pacheco, L. Ciriaco and A. Lopes. Anodic oxidation of a biologically treated leachate on a boron-doped diamond anode. *J. Hazard. Mater.* 199-200 (2012) 82-87.
- [6] D. Norma, A. Fernandes, L. Ciriaco, M.J. Pacheco, A. Lopes. Electrocoagulation and Anodic Oxidation as a Complement of Biological Treatment of Sanitary Landfill Leachates. *Port. Electroch. Acta* 30 (2012) 281-294.
- [7] Eaton, A., Clesceri, L., Greenberg, A., 2005. Standard methods for examination of water and wastewater, 21st Ed., APHA, AWWA, WEF, Washington.
- [8] Liu H, Zhao X, Qu J. Electrocoagulation in water treatment. In:Comninellis C, Chen G, ed.. *Electrochemistry for the environment*. NewYork. Springer Science+Business Media, LLC; 2010.

Acknowledgement

Financial support from FEDER, Programa Operacional Factores de Competitividade – COMPETE and FCT, for the projects PTDC/AAC-AMB/103112/2008, PEst-OE/CTM/UI0195 /2011 of the MT&P Unit and grant SFRH/BD/81368/2011